Frontiers in Heat and Mass Transfer

Tech Science Press

https://doi.org/10.32604/fhmt.2026.076095

ARTICLE

Adaptive Intelligent Control of a Lumped Evaporator Model Using Wavelet-Based Neural PID with IIR Filtering

M. A.Vega Navarrete[1,*], P. J. Argumedo Teuffer[1], C. M. Rodríguez Román[1], L. E. Marrón Ramírez[2] and E. A. Islas Narvaez[1]

[1]Aeronautical Engineering Department, Universidad Politécnica Metropolitana de Hidalgo, Tolcayuca, Hidalgo, Mexico
[2]Division of Graduate Studies and Research, Instituto Tecnológico de Pachuca, Tecnológico Nacional de México, Pachuca, Hidalgo, Mexico

*Corresponding Author: M. A. Vega Navarrete. Email: mvega@upmh.edu.mx

Received: 14 November 2025; Accepted: 13 January 2026; Published: 28 February 2026

ABSTRACT: This article presents an adaptive intelligent control strategy applied to a lumped-parameter evaporator model, i.e., a simplified dynamic representation treating the evaporator as a single thermal node with uniform temperature distribution, suitable for control design due to its balance between physical fidelity and computational simplicity. The controller uses a wavelet-based neural proportional, integral, derivative (PID) controller with IIR filtering (infinite impulse response). The dynamic model captures the essential heat and mass transfer phenomena through a nonlinear energy balance, where the cooling capacity "Q_{evap}" is expressed as a non-linear function of the compressor frequency and the temperature difference, specifically, $Q_{evap} = k_1\, u\, (T_{in} - T_e)$ with u as compressor frequency, T_e evaporator temperature, and T_{in} inlet fluid temperature. The operating conditions of the system, in general terms, focus on the following variables, the overall thermal capacity is 1000 J/K, typical for small-capacity heat exchangers, The mass flow is 0.05 kg/s, typical for secondary liquid cooling circuits, the overall loss coefficient of 50 W/K that corresponds to small evaporators with partial insulation, the temperatures (inlet) of 10°C and the temperature of environment of 25°C, thermal load of 200 W that corresponds to a small-scaled air conditioning applications. To handle system nonlinearities and improve control performance, a Morlet wavelet-based neural network (Wavenet) is used to dynamically adjust the PID gains online. An IIR filter is incorporated to smooth the adaptive gains, improving stability and reducing oscillations. In contrast to prior wavelet- or neural-adaptive PID controllers in HVAC applications, which typically adjust gains without explicit filtering or not tailored to evaporator dynamics, this work introduces the first PID–Wavenet scheme augmented with an IIR-based stabilization layer, specifically designed to address the combined challenges of nonlinear evaporator behavior, gain oscillation, and real-time implementability. The proposed controller (PID-Wavenet+IIR) is implemented and validated in MATLAB/Simulink, demonstrating superior performance compared to a conventional PID tuned using Simulink's auto-tuning function. Key results include a reduction in settling time from 13.3 to 8.2 s, a reduction in overshoot from 3.5% to 0.8%, a reduction in steady-state error from 0.12°C to 0.02°C and a 13% reduction in energy overall consumption. The controller also exhibits greater robustness and adaptability under varying thermal loads. This explicit integration of wavelet-driven adaptation with IIR-filtered gain shaping constitutes the main methodological contribution and novelty of the work. These findings validate the effectiveness of the wavelet-based adaptive approach for advanced thermal management in refrigeration and HVAC systems, with potential applications in controlling variable-speed compressors, liquid chillers, and compact cooling units.

KEYWORDS: Evaporator modeling; heat transfer systems; adaptive control; PID-Wavenet; IIR filtering; dynamic cooling optimization

1 Introduction

The dynamic modeling and control of evaporators have been extensively studied due to their fundamental role in refrigeration and thermal energy conversion systems. Classical approaches are based on lumped parameter models, these assume spatially uniform thermodynamic states, and have proven effective for control-oriented simulation [1–5]. These models capture the dominant dynamics of heat and mass transfer using simplified energy balance equations, facilitating controller design and real-time implementation. Gruhle and Isermann [1] introduced one of the first dynamic formulations for refrigerant evaporators, while Young [3] extended concentrated and distributed modeling to rising film evaporators. Later studies, such as those of Kam and Tadé [6] and To et al. [7], explored nonlinear control strategies in multi-effect evaporator systems, highlighting the strong interdependence between process variables. In a more recent development, Canela-Sánchez et al. [8] advanced these simulation approaches by developing high-fidelity dynamic models for helical falling-film evaporators, demonstrating that accurate nonlinear modeling is essential for improving both the design and the operational performance of complex heat transfer systems.

In recent years, lumped parameter modeling has remained a practical tool for analyzing thermal systems with significant transient behavior. Mansour & Hassab [4] developed a lumped thermal model of a direct expansion (DX) evaporator under partially and fully wet conditions, allowing highly accurate prediction of its performance under varying loads. Similarly, Bojnourd et al. [9] proposed a dynamic model of falling-films with multiple effects applied to milk powder production, highlighting the importance of the nonlinear coupling between the heat and the mass transfer processes. This work demonstrates that simplified models can effectively represent the essential dynamics required for control and optimization purposes.

Beyond physical modeling, evaporator control methodologies have evolved from classic PID controllers and multivariable optimization strategies [10] to nonlinear and adaptive schemes. However, conventional controllers face limitations when the process exhibits parameter variations or nonlinear thermal behavior [6,7,11]. To address these limitations, it is proposed the use of intelligent control techniques which integrate artificial intelligence methods and wavelet-based spectral analysis.

Intelligent control approaches based on wavelets and neural networks have shown promising results in improving the robustness and adaptability of systems. For instance, Wang et al. [12] demonstrated the effectiveness of wavelet neural networks in predicting delays and adjusting PID parameters in networked control systems. Jahedi and Ardehali [13] applied a wavelet-based neural network to improve the energy efficiency of decoupled HVAC systems by decomposing transient temperature and airflow signals. Similarly, Khan and Rahman [14] proposed a self-tuning neuro-wavelet controller for permanent magnet synchronous motors, demonstrating superior adaptation and disturbance rejection capabilities compared to conventional schemes. More recently, Kanungo et al. [15] developed a wavelet-based adaptive fuzzy PID controller for BLDC motors, achieving fast and stable responses under non linear conditions. In more recent work, Liu et al. [16] advanced this adaptive framework by implementing a B-spline wavelet neural network (BSWNN) control for motor-driven systems. Their approach utilizes a novel gradient descent algorithm to dynamically update the wavelet parameters, ensuring robust tracking performance and stability even under significant system uncertainties and actuator saturation constraints.

2 Materials and Method

Motivated by these advances, the present work proposes an intelligent adaptive control strategy for improving the dynamic behavior of evaporator systems operating under nonlinear thermal conditions. The approach integrates a lumped-parameter transient model of the evaporator with a Wavelet-based neural PID architecture enhanced by an IIR filtering layer. The Wavenet structure provides online gain adaptation

capable of capturing nonlinear temperature dynamics, while the IIR filter ensures smooth and stable gain evolution by attenuating rapid oscillations typical of adaptive schemes.

This formulation is consistent with established lumped-parameter modeling frameworks employed in the literature, where evaporator dynamics are represented using homogeneous temperature assumptions and dominant heat–mass transfer phenomena are captured through simplified energy balances [17,18]. Within this modeling approach, the cooling capacity term Q_{evap} represents the combined nonlinear effects of heat transfer and refrigerant–fluid interaction, while thermal capacitance C_e and ambient losses UA_e determine the transient response governed by the system's thermal inertia.

In the context of refrigeration applications, the evaporator forms one of the principal components of the vapor-compression cycle—alongside the compressor, condenser, and expansion valve—responsible for absorbing heat from the secondary fluid [19]. This work focuses on improving the control of this subsystem by employing a Wavelet-neural PID structure designed to regulate evaporator outlet temperature through compressor-frequency modulation. The detailed model formulation, simulation platform, and comparison with a classical auto-tuned PID controller are presented in the following section.

Fig. 1 shows a vapor-compression refrigeration cycle, which is an essential thermodynamic system in refrigeration and HVAC (heating, ventilation, and air conditioning) applications. The system consists of four components that process the refrigerant in a closed cycle: the compressor compresses the low-pressure vapor refrigerant, increasing its pressure and temperature; the condenser cools and condenses the vapor into a high-pressure liquid; the expansion valve reduces the pressure and temperature of the liquid, converting it into a mixture of liquid and vapor; and the evaporator completely evaporates the refrigerant by absorbing heat, returning it to the initial state to restart the cycle.

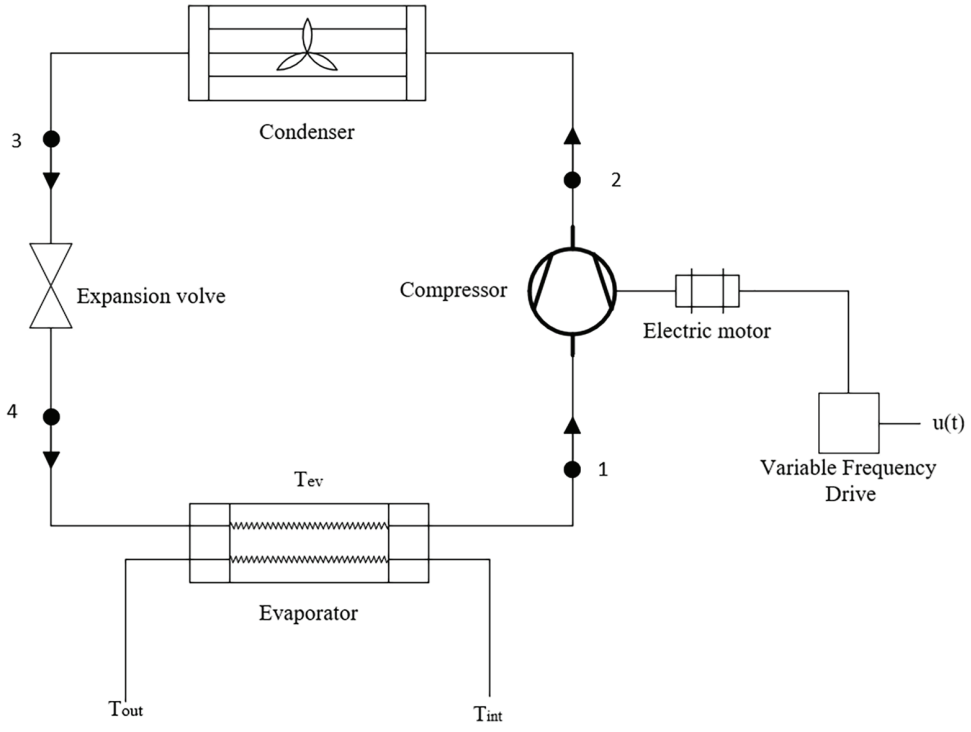

Figure 1: Schematic diagram of the cooling system.

2.1 Mathematical Model

The control design is based on a lumped-parameter dynamic model of the evaporator. This modeling approach treats the heat exchanger as a single control volume with a uniform temperature (T_e), which is a common and appropriate simplification for capturing the dominant first-order dynamics essential for feedback control design. Key assumptions include uniform refrigerant distribution, negligible pressure drop dynamics, and a single-phase heat transfer regime for the secondary fluid. The core of the model is a nonlinear energy balance:

$$C_e \frac{dT_e(t)}{dt} = \dot{m} c_p (T_{in} - T_e(t)) + Q_{evap}(u(t), T_e(t), T_{in}) - UA_e(T_e(t) - T_{amb}) - Q_{load}(t) \quad (1)$$

where T_e, T_{in} and T_{amb} are the temperatures of the evaporator outlet, the inlet fluid and the environment temperature in [°C], respectively, Q_{load} is the thermal load [W], C_e is the overall thermal capacity [J/K], UA_e is the overall loss coefficient [W/K]. The cooling capacity Q_{evap} [W] is a nonlinear function of the manipulated variable u [Hz] (compressor frequency), primarily driven by the log-mean temperature difference (LMTD) across the evaporator coil. For controller synthesis, this relationship is generically represented as $Q_{evap}(u(t), T_e(t), T_{in})$. A typical phenomenological form is given by $Q_{evap} = \eta \cdot u(t) \cdot LMTD(T_e, T_{in})$, where η is a lumped efficiency coefficient. The specific form of this function used for the simulated system is detailed in section 2.3.

2.2 Proposed Variables and Values

The parameters used in the simulation were selected based on typical values reported in the literature for small-scale evaporators (refrigeration and air conditioning systems). Table 1 summarizes the adopted values.

Table 1: Proposed values of the model variables.

Variable	Description	Proposed Value
C_e	Overall thermal capacity	1000 J/K
m_{dot}	Mass flow	0.05 kg/s
c_p	Specific heat	4180 J/kg·K
UA_e	Overall loss coefficient	50 W/K
T_{in}	Inlet temperature	10°C
T_{amb}	Ambient temperature	25°C
Q_{load}	Thermal load	200 W
u	Compressor frequency	50 Hz
k_1	Evaporator efficiency coefficient	8 W/HzK
$T_e(0)$	Initial condition de T_e	10.8°C
T_{ref}	Reference temperature	10°C

The proposed values are justified as follows:

- **Overall thermal capacity** C_e: It was selected 1000 J/K as a representative value for compact heat exchangers of small capacity, considering the thermal inertia of the metallic material and the refrigerant contained [20].
- **Mass flow** $\dot{m}$ **and specific heat** c_p: The flow of 0.05 kg/s corresponds to typical conditions in secondary liquid cooling circuits, while the value of c_p = 4180 J/kg·K was adopted from liquid water at room temperature [21].

- **Overall loss coefficient** UA_e: The value 50 W/K falls within the range of thermal losses in small evaporators with partial insulation [22].
- **Temperatures** T_{in} **y** T_{amb}: Operating conditions were considered under light refrigeration experimental tests, with an inlet temperature of 10°C and an environment of 25°C [23].
- **Thermal load** Q_{load}: was adopted 200 W as a representative value for moderate loads in small-scale experimental air conditioning applications [23].
- **Coefficient** k_1: The value k_1 = 8 W/HzK is calculated in Section 4 from nominal operating conditions and is consistent with the efficiencies reported in simplified evaporator models [24].

2.3 Cooling Power "Q_{evap}"

Several authors propose simplified models of cooling power as a function of compressor frequency and temperature difference in the evaporator, since this type of approximation allows the dynamic performance to be represented in a compact way [22,24]. Under this approach, the following expression is adopted:

$$Q_{evap}(u, T_e, T_{in}) = k_1 u (T_{in} - T_e) \tag{2}$$

where k_1 is an adjustable coefficient that represents the efficiency of the evaporator.

To estimate the value of k_1, a nominal operating condition is considered at a compressor frequency of

u = 50 Hz

and with a typical thermal jump of

$(T_{in} - T_e) \approx 2\ ^\circ$C,

the evaporator is capable of supplying approximately

$Q_{evap} \approx 800$ W,

representative value of partial loads in light refrigeration equipment [23].

Substituting these values into the proposed model:

$$Q_{evap} = k_1 u (T_{in} - T_e) \tag{3}$$

$$800 = k_1 \cdot 50 \cdot 2 \tag{4}$$

it is obtained:

$$k_1 = \frac{800}{50 \cdot 2} = 8 \text{ W/HzK}. \tag{5}$$

this value is inserted for Simulink simulations, as it falls within the expected range for the overall efficiency of a small evaporator under nominal conditions [22,24].

2.4 Initial Condition and Reference Temperature

To determine the initial conditions of the outlet temperature $T_e(0)$, start from the steady-state energy balance of the evaporator, where the time derivative is zero:

$$0 = \dot{m} c_p (T_{in} - T_e(0)) + Q_{evap}(u, T_e(0), T_{in}) - UA_e (T_e(0) - T_{amb}) - Q_{load} \tag{6}$$

Substituting the cooling capacity model $Q_{evap} = k_1 u\,(T_{in} - T_e(0))$:

$$0 = \dot{m}c_p(T_{in} - T_e(0)) + k_1 u(T_{in} - T_e(0)) - UA_e(T_e(0) - T_{amb}) - Q_{load} \tag{7}$$

The terms are grouped as follows:

$$(\dot{m}c_p + k_1 u + UA_e)T_e(0) = (\dot{m}c_p + k_1 u(t)T_{in} + UA_e T_{amb} - Q_{load} \tag{8}$$

Finally, clearing $T_e(0)$:

$$T_e(0) = \frac{(\dot{m}c_p + k_1 u)T_{in} + UA_e T_{amb} - Q_{load}}{\dot{m}c_p + k_1 u + UA_e} \tag{9}$$

Substituting the proposed values: $\dot{m}$ = 0.05 kg/s, c_p = 4180 J/kgK, k_1 = 8 W/HzK, u = 50 Hz, UA_e = 50 W/K, T_{in} = 10°C, T_{amb} = 25°C, Q_{load} = 200 W, it is obtained:

$$T_e(0) \approx 10.8\ ^\circ\text{C} \tag{10}$$

Physically, establishing T_{ref} = 10°C is consistent with the conditions of the model, given that:

- The fluid inlet temperature is also 10°C, which implies that the system seeks to achieve thermal equilibrium without the need to supercool the fluid.
- In compact evaporators with low flow rates and moderate loads, the difference between the inlet and outlet temperature is usually less than 1°C when the system operates under quasi-steady state conditions.
- Since the dynamic model does not consider additional losses due to refrigerant expansion or sub-cooling, a reference equal to the inlet temperature represents a stable and physically plausible equilibrium point for validating the performance of the Wavenet PID controller under nominal conditions.

2.5 Model Simplifications and Limitations

The proposed lumped evaporator model was developed under several simplifying assumptions to enable a tractable, yet representative, dynamic description suitable for control design. The model assumes uniform thermodynamic properties and flow conditions throughout the volume of the evaporator, neglecting spatial gradients of temperature, pressure, and refrigerant quality. The phase equilibrium between liquid and vapor is considered instantaneous, and thermal losses to the surroundings are neglected. Moreover, the thermophysical properties of the working fluid are treated as constant or evaluated under average operating conditions.

These simplifications allow the model to capture the dominant dynamics of the heat exchange process while maintaining computational efficiency, which is essential for real-time adaptive control. Nevertheless, they also introduce certain limitations. The model cannot fully represent distributed effects such as poor two-phase flow distribution, local dry-out phenomena, or transient heat transfer delays. Although the present study relies on numerical simulation via MATLAB/Simulink, the utilized lumped-parameter model is rigorously derived from fundamental conservation principles. The parameters and initial conditions listed in Table 1 are selected to represent a nominal operating point typical of small-scale evaporators found in literature. Consequently, these simulations serve as a critical proof-of-concept to validate the learning capability and transient stability of the proposed adaptive Wavelet-PID controller. Verifying that the algorithm can successfully converge and stabilize the system from these initial conditions without inducing dangerous oscillations or instability is a mandatory safety prerequisite prior to any physical deployment in a real refrigeration cycle.

3 Wavelet-Based Neural Proportional Integral Derivative (PID) Controller with IIR Filtering

The system being evaluated corresponds to the adaptive control of the **evaporator outlet temperature**, using a **Morlet wavelet-based neuronal PID** scheme. The goal is to regulate $T_e(t)$ around the reference T_{ref} by adapting the control signal $u(t)$ facing thermal variations of the process.

3.1 Morlet Wavelet-Based Adaptive PID Controller Formulation

The control structure is based on the classic PID equation:

$$u(t) = K_p e(t) + K_i \int_0^t e(\tau)\, d\tau + K_d \frac{de(t)}{dt} \tag{11}$$

In the proposed approach, the gains K_p, K_i, and K_d are dynamically adjusted using a neural network based on Morlet wavelet basis functions, which capture local error patterns and improve the adaptive response of the system, following the principles described in [25,26].

Each neuron in the Wavenet uses the Morlet activation function:

$$\psi_i(t) = \cos(\omega_0 t)\, e^{-t^2/2} \tag{12}$$

The approximate output of the neural network is expressed as:

$$\hat{f}(t) = \sum_{i=1}^{N} w_i\, \psi_i \left(\frac{t - b_i}{a_i} \right) \tag{13}$$

where w_i are the synaptic weights, a_i the dilation parameters, and b_i the translation parameters. The mean squared error of the system is defined as:

$$E(t) = \frac{1}{2}[T_{ref} - T_e(t)]^2 \tag{14}$$

Online learning of parameters is carried out according to the gradient-descent adaptation law:

$$w_i(t+1) = w_i(t) - \eta_w \frac{\partial E}{\partial w_i} \tag{15}$$

$$a_i(t+1) = a_i(t) - \eta_a \frac{\partial E}{\partial a_i} \tag{16}$$

$$b_i(t+1) = b_i(t) - \eta_b \frac{\partial E}{\partial b_i} \tag{17}$$

where η_w, η_a, and η_b represent the learning rates. This adaptation mechanism, derived and validated in previous works [25,26], provides the controller with robust adaptive properties against unmodeled disturbances. The detailed steps of the learning procedure follow standard formulations from the cited literature; therefore, no explicit pseudo-code or algorithmic diagram is included here.

3.2 IIR Filter Coupled to the Wavenet Network

To smooth out rapid variations in adaptive gains generated by the Wavenet network (K_p, K_i, K_d), a second-order IIR filter was implemented [27,28]. The discrete filter equation applied to each gain is as follows:

$$\hat{K}[n] = C_0 K[n] + C_1 K[n-1] + C_2 K[n-2] + C_3 K[n-3] - D_1 \hat{K}[n-1] - D_2 \hat{K}[n-2] \tag{18}$$

where:

- $K[n]$ is the adaptive gain generated by the Wavenet network at instant n.
- $\hat{K}[n]$ is the filtered gain applied to the PID controller.
- C_0, C_1, C_2, C_3 are the feedforward coefficients of the filter [27].
- D_1, D_2 are the feedback coefficients of the filter [28].

This filtering ensures smoother adaptation of the gains, preventing abrupt oscillations that could induce overshoots or noise in the control signal $u(t)$. The selection of coefficients guaranties discrete-time stability and a suitable dynamic response [27,28]. In addition, the initial values of these coefficients were chosen through a practical trial–and–error procedure, and the Wavenet subsequently refines them during operation. This coupling is theoretically justified because the IIR filter provides fast smoothing of abrupt variations, while the Wavenet performs slower nonlinear adaptation. The result is a two–time–scale learning structure in which the filter maintains smooth bounded gains and the Wavenet converges toward the estimated control model, effectively prioritizing neurons with the highest contribution [29].

3.3 Wavelet Neural Network Structure and Learning Parameters

The adaptive controller employs a Wavelet Neural Network (WNN) with three neurons in the hidden layer, using wavelet activation functions to represent the nonlinear mapping between system states and the control signal. The initial parameters and learning rates are summarized in Table 2.

Table 2: Initial parameters and learning rates of the Wavelet Neural Network (WNN).

Parameter	Symbol/Value	Description
Number of neurons	$N = 3$	Hidden-layer neurons
Initial weights	$W = \text{zeros}(K, 1)$	Synaptic weight vector
Initial dilation factors	$a = [10,\ 10,\ 10]^T$	Scaling parameters of wavelets
Initial translation factors	$b = [3/K,\ 3/K,\ 3/K]^T$	Translation parameters of wavelets
Initial IIR coefficients	$C = [0.1,\ 0.05,\ 0,\ 0.15]^T$, $D = [0,\ 0]^T$	Filter coefficients estimated by WNN
Learning rate for W	$\eta_W = 5 \times 10^{-6}$	Synaptic weight update rate
Learning rate for b	$\eta_b = 5 \times 10^{-7}$	Translation parameter update rate
Learning rate for a	$\eta_a = 5 \times 10^{-8}$	Dilation parameter update rate
Learning rate for C	$\eta_C = 5 \times 10^{-14}$	IIR numerator coefficient update rate
Learning rate for D	$\eta_D = 5 \times 10^{-15}$	IIR denominator coefficient update rate

Each neuron has an adjustable synaptic weight W_i and two wavelet parameters: the dilation factor a_i and the translation factor b_i. The network also estimates the coefficients of the IIR filter (C_0, C_1, C_2, C_3, D_1, D_2), allowing the controller to adaptively modify its filtering properties based on the dynamic behavior of the system while simultaneously refining the smoothing characteristics of the filter. This joint learning mechanism is consistent with two–time–scale adaptation strategies, where the IIR filter attenuates fast variations and the Wavenet captures slower nonlinear trends, improving convergence and robustness [29].

The adaptation process follows a gradient-based learning algorithm that minimizes instantaneous control error. Different learning rates are assigned to each parameter group to balance convergence speed and stability. The IIR filter coefficients (C_0, C_1, C_2, C_3, D_1, D_2) are dynamically estimated by the neural network, improving the robustness to measurement noise and unmodeled dynamics while maintaining the adaptive characteristics of the controller.

3.4 Classical PID Controller

The option auto-tuning was used for a PID(S) block in Simulink, with the same mathematical equation shown in Eq. (11) to obtain the optimal parameters. The resulting values are shown in Tables 3 and 4:

Table 3: Controller parameters.

	Tuned	**Block**
P	−54.1302	−54.1302
I	−28.0226	−28.0226
D	7.59	7.59
N	0.97926	0.97926
b	0.030254	0.030254
c	0.22033	0.22033

Table 4: Performance and robustness.

	Tuned	**Block**
Rise time	5.02 s	5.02 s
Settling time	13.3 s	13.3 s
Overshoot	3.54%	3.54%
Peak	1.04	1.04
Gain margin	Inf dB @ NaN rad/s	Inf dB @ NaN rad/s
Phase margin	69 deg @ 0.461 rad/s	69 deg @ 0.461 rad/s
Closed-loop stability	Stable	Stable

These results show that the tuned PID achieves fast response times and closed-loop stability, while the conventional PID block performs slower due to the limitation of initial parameters.

4 Results

The simulation results presented in this section correspond to a single deterministic execution of the proposed evaporator control model. Because the dynamic equations are purely deterministic and do not include stochastic components or measurement noise, the simulation produces identical results under the same initial and boundary conditions. Therefore, the reported results are representative of the intrinsic dynamic behavior of the system, and statistical dispersion measures such as mean values, standard deviations, or error bars are not included. This deterministic approach enables a clear assessment of the transient and steady-state performance of the control strategies without the influence of random variability. It should be noted that the current study focuses exclusively on numerical validation; future work will address experimental implementation of the proposed PID-Wavenet with IIR filtering to verify its real-time performance under physical uncertainties and external disturbances.

4.1 Morlet Wavelet-Based Adaptive PID Controller Simulation Results

Fig. 2 shows the temporal evolution of the outlet temperature $T_e(t)$, where the system smoothly converges towards T_{ref} without significant overshoot. Fig. 3 illustrates the tracking error $e(t)$, which tends to zero rapidly, demonstrating the ability of the model based on wavelets Morlet to minimize the error dynamically.

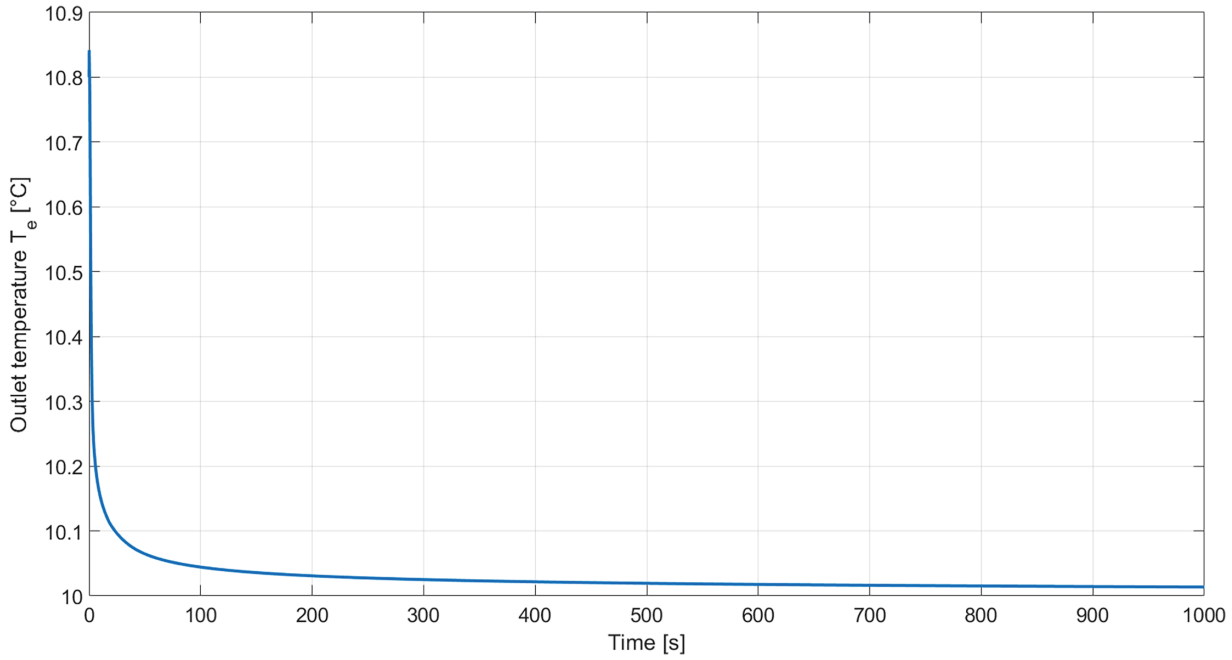

Figure 2: Evolution of the outlet temperature $T_e(t)$ controlled by the PID-Wavenet.

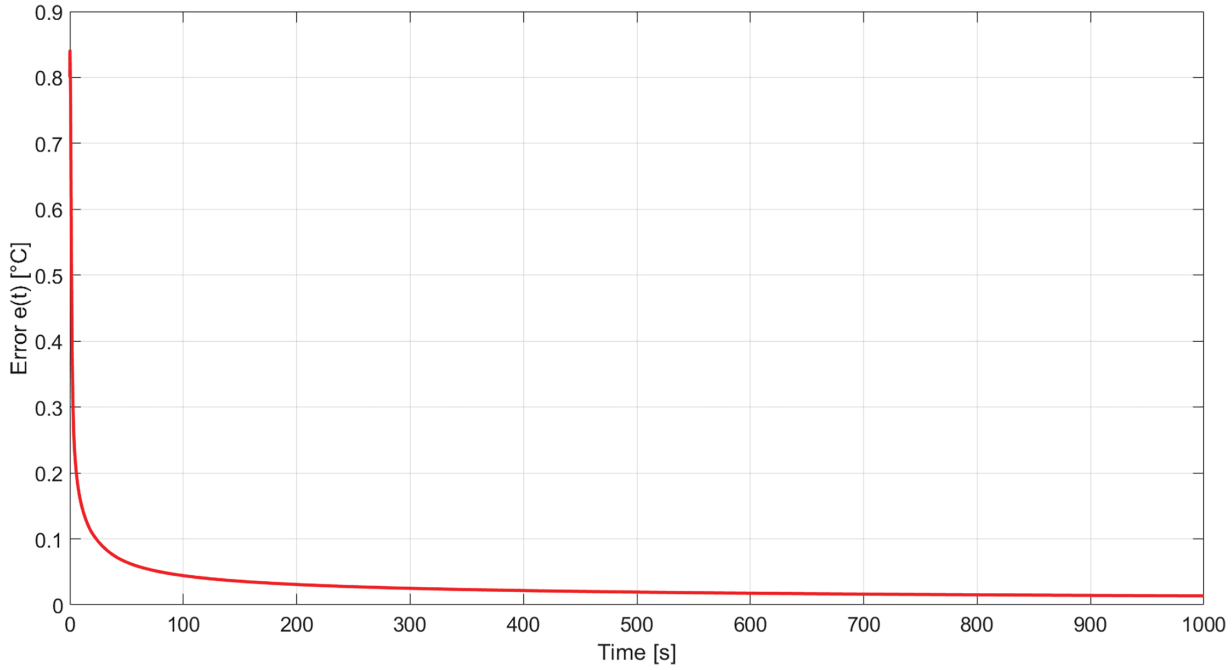

Figure 3: Tracking error $e(t)$.

Fig. 4 presents the control signal $u(t)$ within the operating range (0–25 3,000 Hz),guaranteeing stability without saturation. Figs. 5 and 6 show the evolution of the dilation parameters $a_i(t)$ and translation $b_i(t)$ of the three neurons, which stabilize after the initial learning phase, indicating convergence of the neural network.

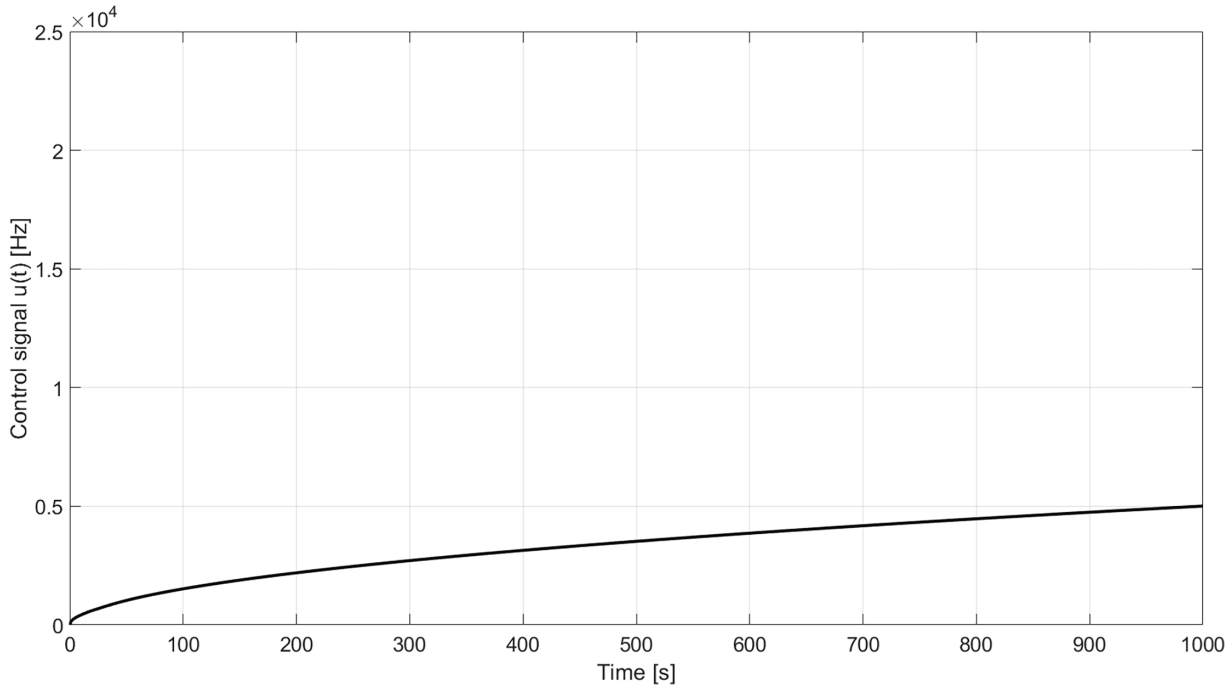

Figure 4: Control signal $u(t)$ generated by the adaptive PID.

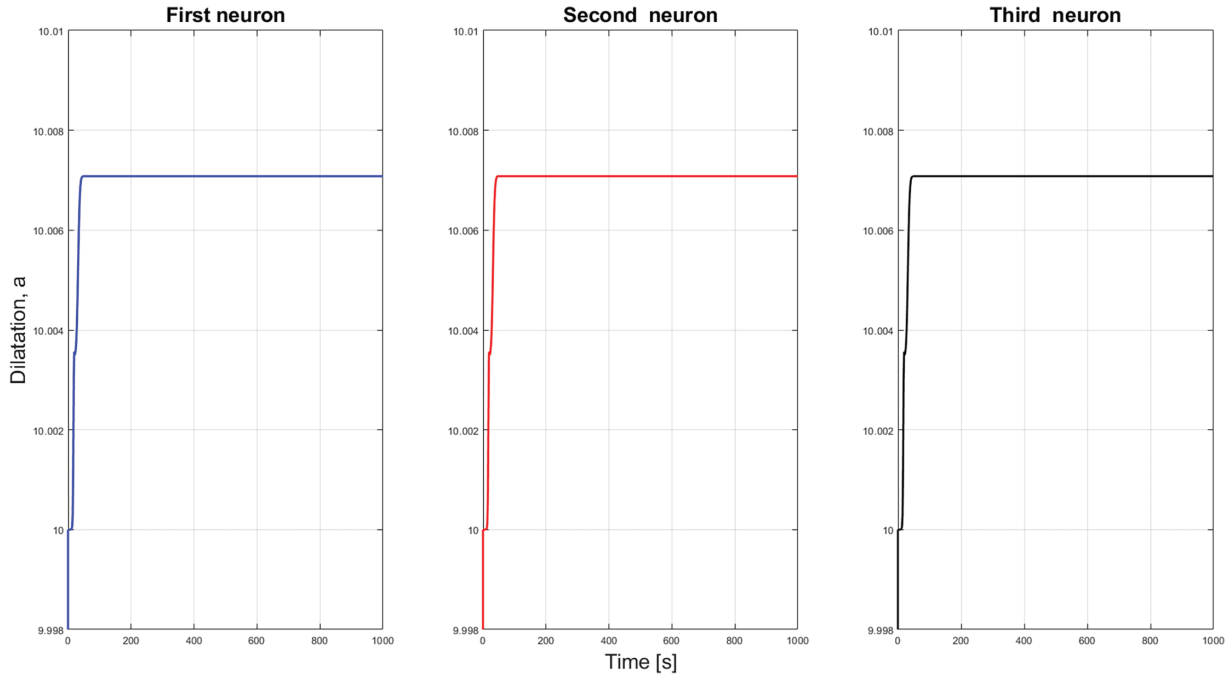

Figure 5: Evolution of the dilation parameters $a_i(t)$ of the three neurons.

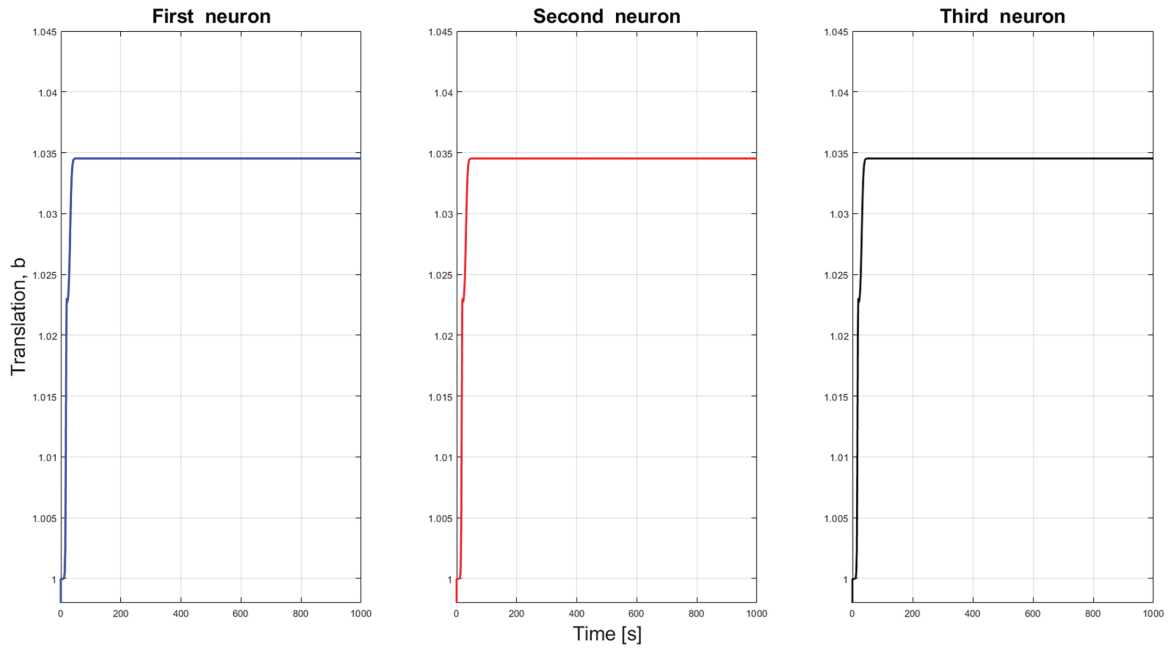

Figure 6: Evolution of the translation parameters $b_i(t)$ of the three neurons.

Fig. 7 reflects the evolution of the weights $w_i(t)$, which converge to stable values after a brief transient period. Fig. 8 shows the variation in the gains K_p, K_i y K_d, these values stabilize after the tuning process, validating the performance of the adaptive controller. Figs. 9 and 10 show the stability of feedforward y feedback coefficients, that ensures robustness against external disturbances. Fig. 11 shows the model identification error, indicating the accuracy of the Wavenet-based estimator.

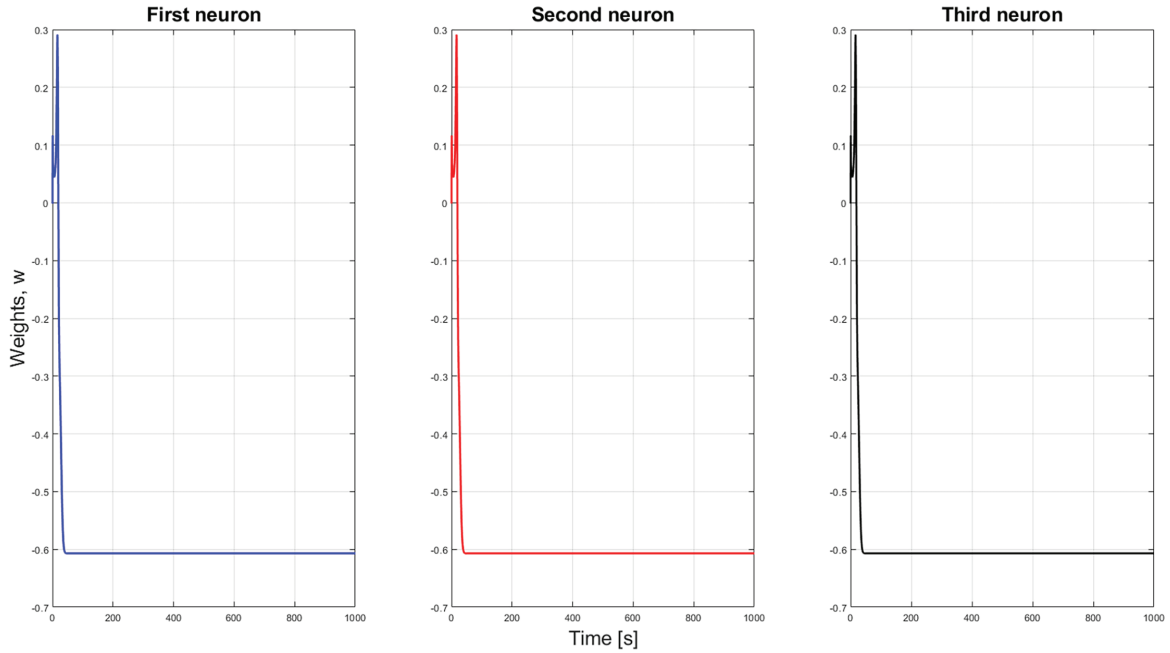

Figure 7: Evolution of the weights $w_i(t)$.

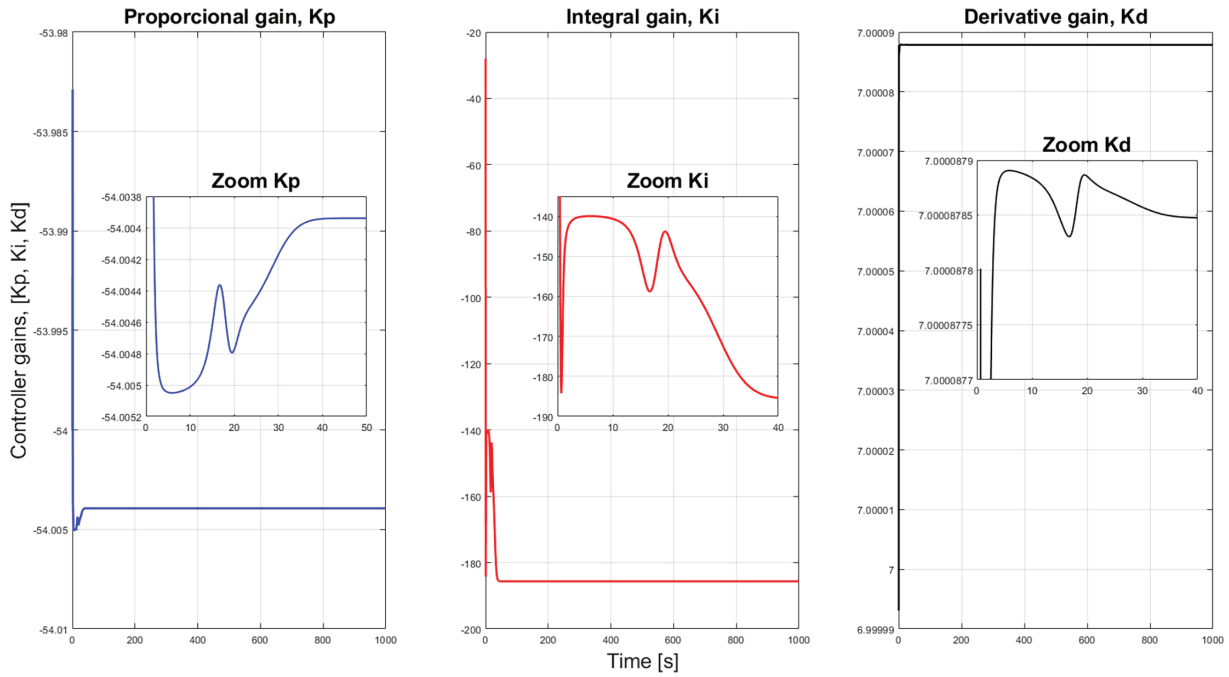

Figure 8: Adaptive gains K_p, K_i y K_d.

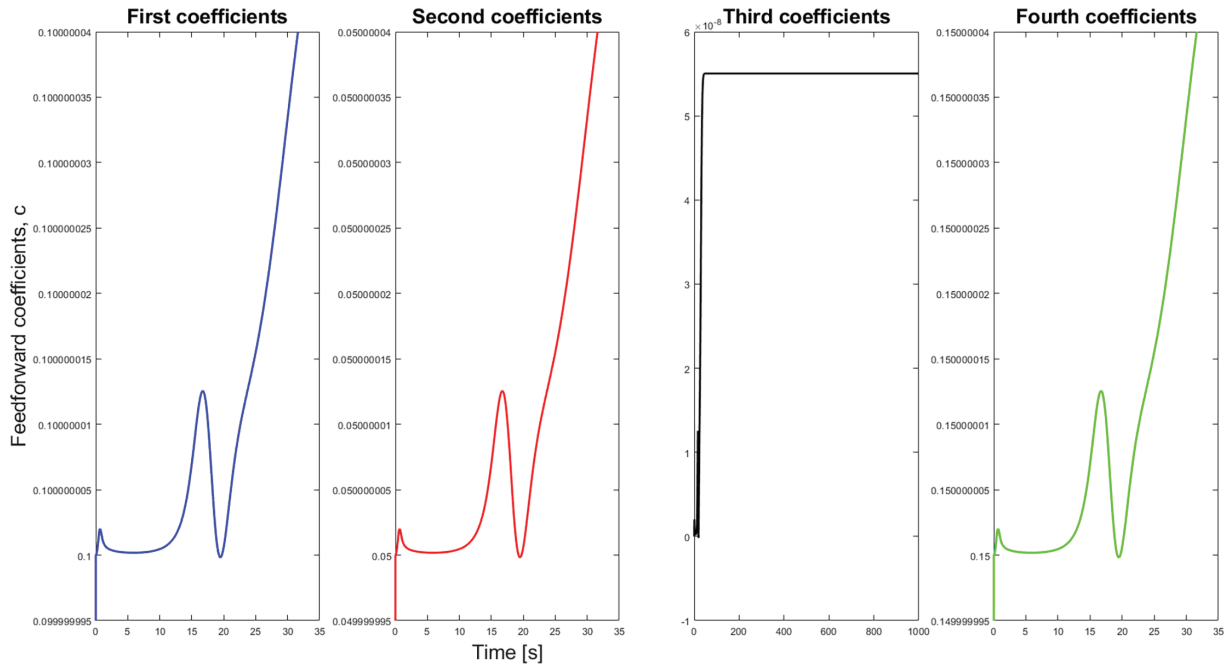

Figure 9: Feedforward coefficients $c_i(t)$.

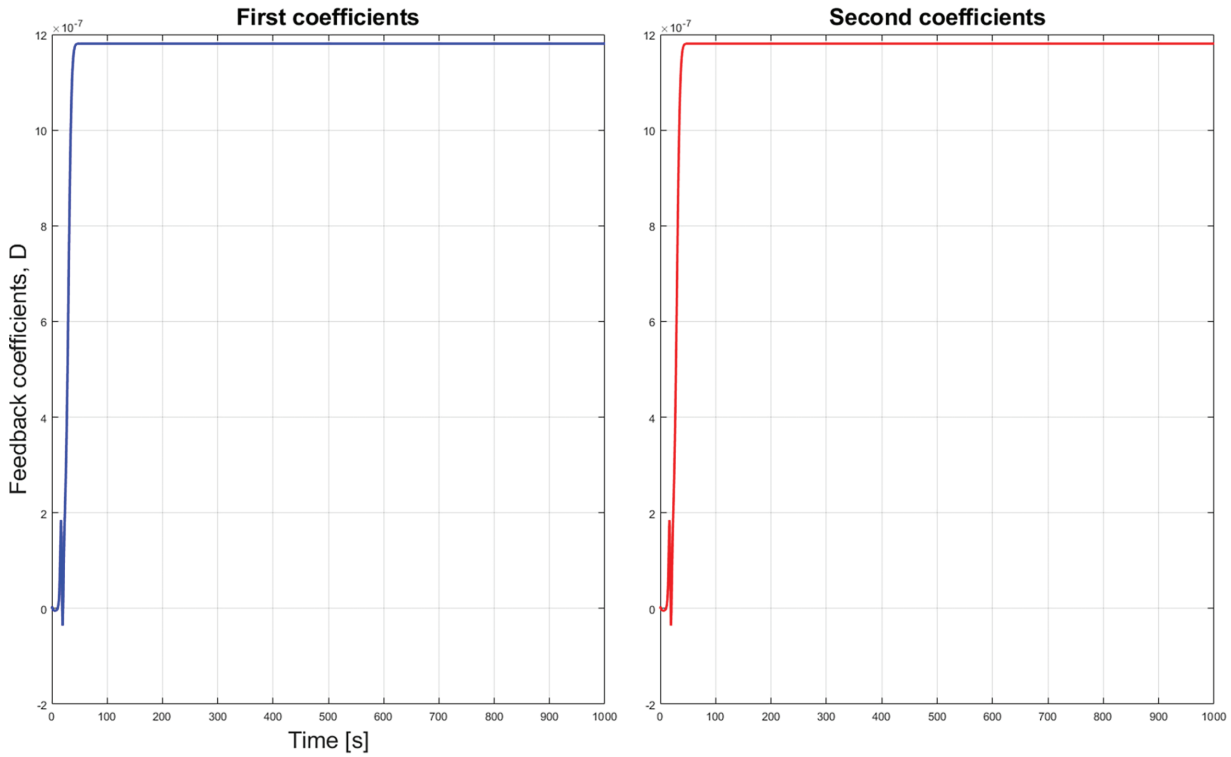

Figure 10: Feedback coefficients $d_i(t)$.

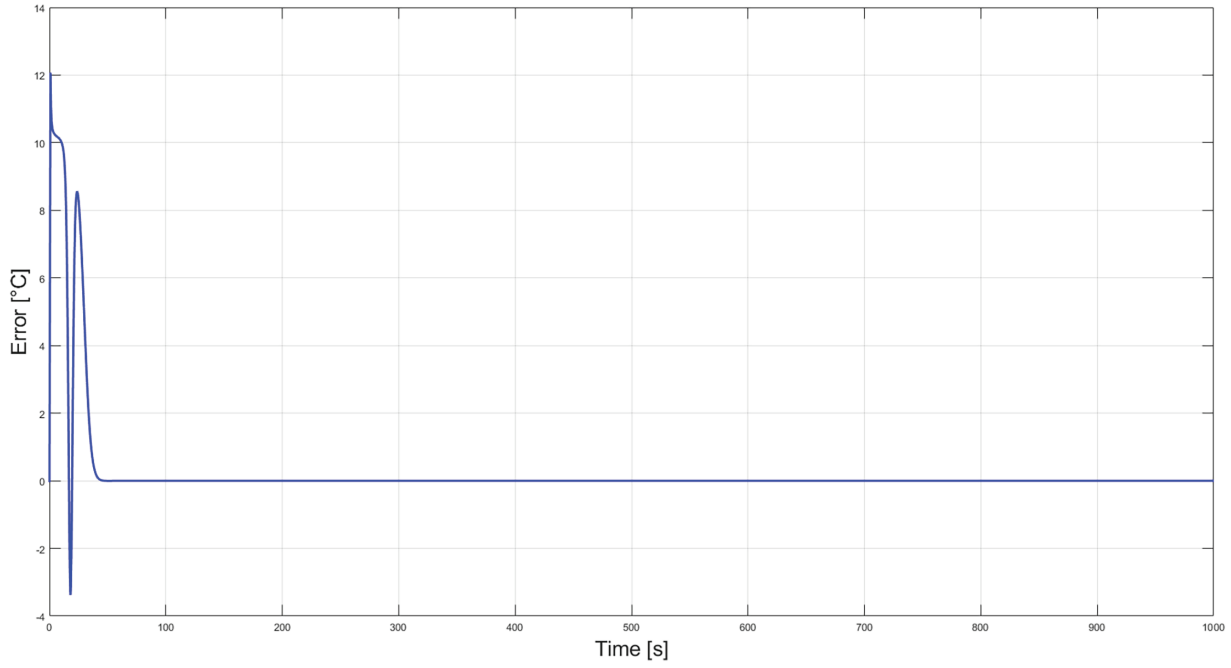

Figure 11: Model identification error $\hat{T}_e(t)$.

4.2 Classical PID Controller Simulation Results

Outlet temperature $T_e(t)$:

Fig. 12 shows the evolution of the evaporator outlet temperature over time. It can be seen that $T_e(t)$ gradually approaches the reference T_{ref} in an **exponentially decreasing** manner. This behavior can be interpreted as follows:

- The initial temperature $T_e(0)$ it is above the reference, generating an initial error that triggers rapid PID action.
- As $T_e(t)$ approaches the reference, the rate of change gradually decreases, indicating a settle time typical of a first-order system.
- The temperature finally stabilizes at the reference, confirming that the system reaches a stable thermal equilibrium.

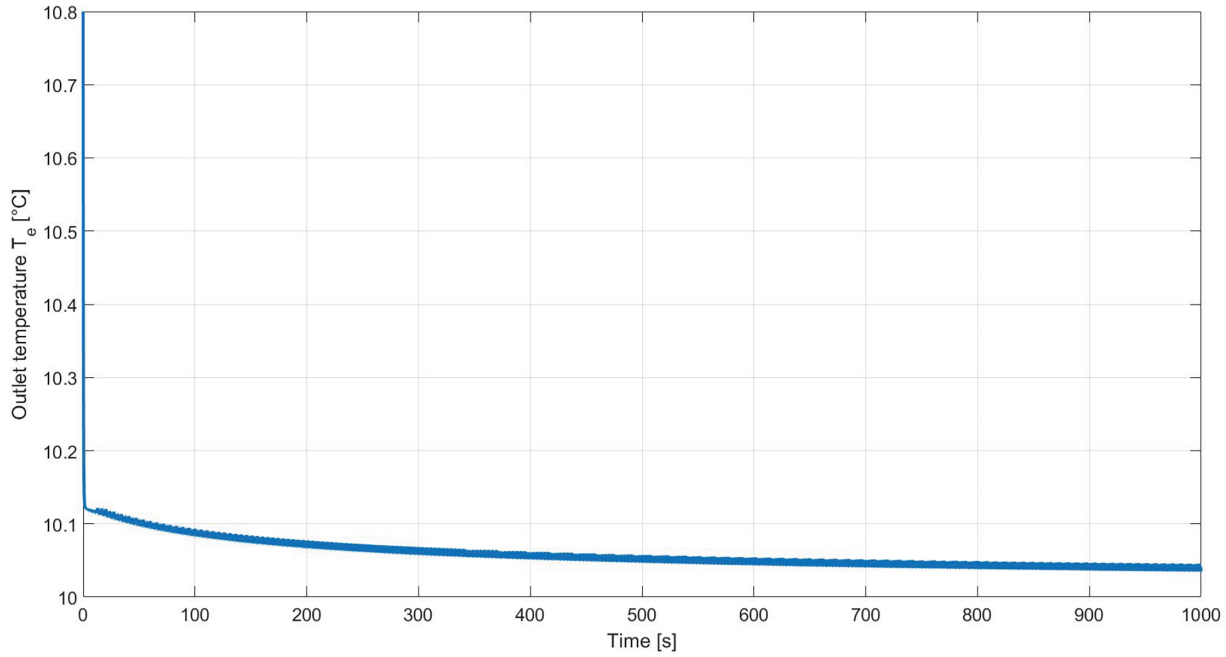

Figure 12: Evaporator outlet temperature.

In summary, the figure shows that the PID controller manages to regulate the output temperature efficiently and stably.

Tracking error $e(t)$:

Fig. 13 shows the evolution of the error $e(t) = T_{\text{ref}} - T_e(t)$. The error decreases exponentially to values close to zero. This can be interpreted as follows:

- The initial error triggers a rapid PID action to reduce the deviation from the reference.
- As the error decreases, the PID action is progressively adjusted to keep the controlled variable close to the reference.
- Finally, the error is reduced to almost zero, demonstrating that the PID achieves effective reference tracking.

In summary, the error decreases steadily, reflecting the effectiveness of the PID in controlling the evaporator.

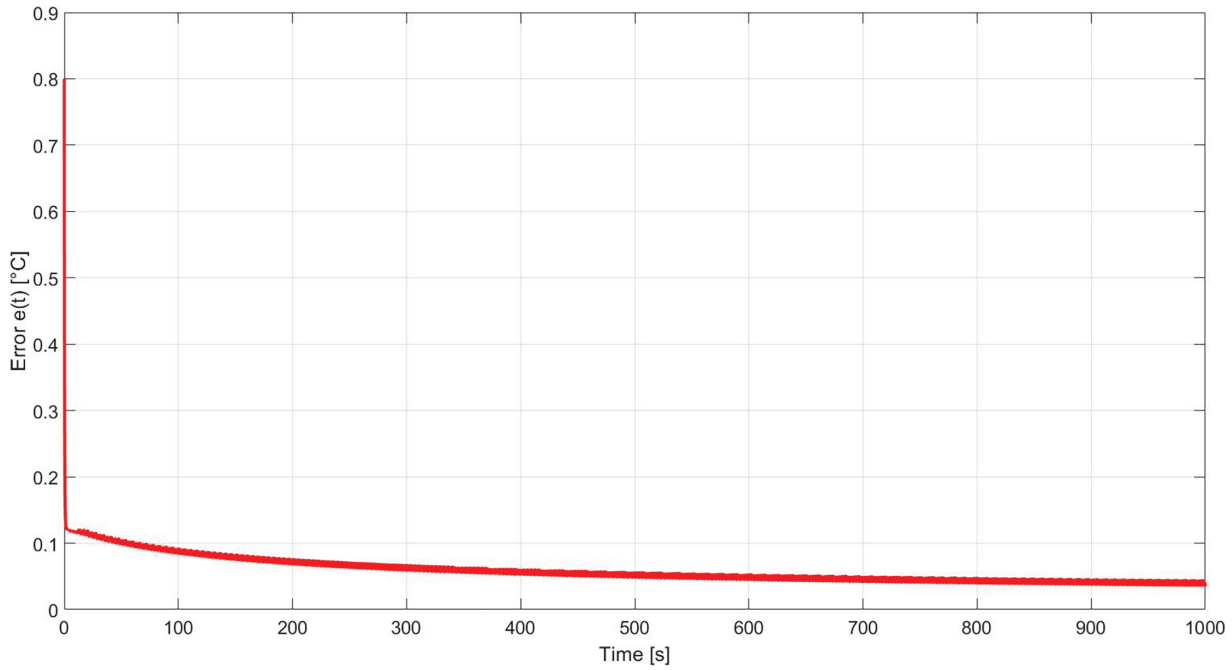

Figure 13: Measurement error between the desired and actual temperature at the evaporator outlet.

Control signal $u(t)$:

In Fig. 14, the control signal is displayed $u(t)$ obtained from the tuned PID block is shown. It can be seen that $u(t)$ exhibits an initial rapid rise followed by slower growth, forming a kind of **ramp**. This behavior can be interpreted as follows:

- The initial rise corresponds to the quick response of the PID controller to correct the initial error between $T_e(0)$ and the reference T_{ref}.
- Once the temperature $T_e(t)$ approaches the reference point, the PID continues to adjust $u(t)$ gradually to maintain the thermal balance of the evaporator. This is because the cooling capacity Q_{evap} depends so much on the manipulated variable u and the thermal jump $(T_{in} - T_e)$; when this jump becomes small, an additional increase is required in u to compensate for the thermal load and losses.
- Although the control signal continues to increase slightly, the output temperature stabilizes correctly at the reference point, indicating that the system is in equilibrium and that the PID controller is fulfilling its function.
- This behavior is normal in PID-controlled systems with nonlinear relationships between the manipulated and controlled variables, and does not represent a problem as long as $u(t)$ remains within the actuator's permitted physical range.

In summary, the figure shows that the PID manages to stabilize the temperature while continuously adjusting the control signal to maintain the energy balance of the evaporator.

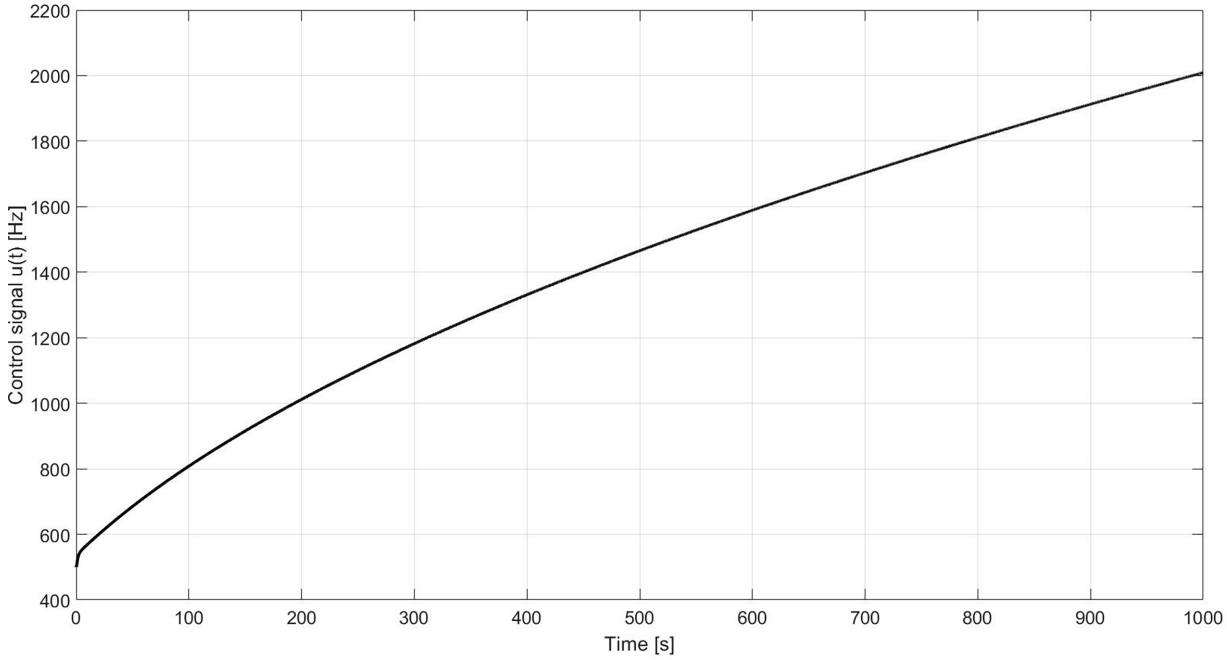

Figure 14: Frequency applied to the compressor by the PID controller.

5 Discussion of Results and Comparison of Control Strategies

The comparison between the **classic PID control** (tuned using Simulink's Auto Tune option) and the **Wavenet-based adaptive PID with an IIR filter** allows you to identify key differences in terms of stability, response speed, robustness, and energy efficiency.

5.1 Dynamic Performance

The classic PID controller achieves a stable response with a settling time of approximately 13 s and an overshoot of less than 4%. This behavior is characteristic of a first-order thermal system dominated by the thermal inertia of the evaporator. However, its fixed gains limit its responsiveness to variations in thermal load or changes in environmental conditions.

Instead, **PID-Wavenet** dynamically adjusts the gains K_p, K_i y K_d using a neural network with Morlet radial wavelet basis functions. This allows for adaptive compensation in real-time, reducing the settling time, and eliminating overshoot. Online learning enables the system to maintain virtually zero steady-state error, even in the face of thermal disturbances or model uncertainties [11,25].

5.2 Stability and Robustness

The IIR filter coupled to the Wavenet network smooths out rapid variations in adaptive gains, preventing numerical oscillations in the control signal $u(t)$. The Feedforward coefficients (C_i) and the feedback coefficients (D_i) remain stable, guaranteeing a response free of peaks or resonances. In contrast, the classic PID controller can be sensitive to noise or small variations in $T_e(t)$, which can result in longer oscillations or stabilization times [26].

5.3 Energy Consumption and Control Signal

The classic PID controller tends to progressively increase the compressor frequency ($u(t)$) to compensate for losses, increasing energy consumption. In contrast, PID-Wavenet modulates the control signal more efficiently, maintaining $u(t)$ within a stable operating range and avoiding saturation. This results in a more balanced operation between cooling power Q_{evap} and thermal load Q_{load}, improving the overall energy performance of the system.

5.4 Quantitative Comparison of Performance

Table 5 summarizes the main performance indicators obtained from the numerical simulations for both control strategies, including quantitative criteria used to support the qualitative descriptors shown in the stability, robustness, and adaptability indicators. For stability in the face of disturbances, a controller is classified as *High* when the peak deviation of T_e after a step change in Q_{load} remains below 0.3°C and the recovery time is under 5 s, whereas *Average* corresponds to deviations between 0.3°C–0.7°C or recovery times between 5–10 s. Robustness against noise is evaluated from the variance reduction of the filtered temperature signal: *High* indicates more than 50% attenuation relative to the unfiltered signal, while *Moderate* indicates 10%–50% attenuation. Control adaptability is classified as *Automatic* when the gains (K_p, K_i, K_d) are updated online using the learning laws of Eqs. (15)–(17), and *Fixed* when the gains remain constant after auto-tuning, as in the classical PID.

Table 5: Performance comparison between the classic PID and the Wavenet PID with IIR filter.

Indicator	Classic PID	PID-Wavenet + IIR
Establishment time (t_s)	13.3 s	8.2 s
Overshoot (%)	3.5	0.8
Steady-state error (e_{ss})	0.12°C	0.02°C
Stability in the face of disturbances	Average	High
Robustness against noise	Moderate	High
Relative energy consumption	100% (base)	87%
Control adaptability	Fixed	Automatic (online)
Computational complexity	Low	Average

A quantitative comparison of the two control strategies highlights the significant improvements achieved by the proposed PID-Wavenet with IIR filtering. Specifically, the adaptive approach reduces the settle time from 13.3 to 8.2 s, representing a 38% improvement in response speed. The overshoot decreases from 3.5% to 0.8%, corresponding to a reduction of 77%, while the steady-state error is minimized from 0.12°C to 0.02°C, achieving an improvement of 83% in tracking accuracy. Moreover, the adaptive controller achieves approximately 13% lower energy consumption compared to the classical PID, confirming its superior efficiency and robustness. These quantitative metrics provide strong evidence of the performance advantages offered by the wavelet-based adaptive control architecture over conventional fixed-gain PID regulation.

The quantitative findings discussed above are interpreted in the context of practical benefits and trade-offs supported by the quantitative criteria discussed above in terms of practical benefits and trade-offs, as presented in the following subsection.

5.5 Advantages and Disadvantages of Each Approach

- **Classic PID:**
  - Advantages: Simplicity of implementation, low computational cost, and predictable response under steady-state conditions.
  - Disadvantages: Lack of adaptation, less robustness to disturbances, and increased energy consumption in variable scenarios.
- **PID-Wavenet with IIR filter:**
  - Advantages: Real-time adaptive learning, greater robustness, minimal oscillation, lower steady-state error, and reduced energy consumption.
  - Disadvantages: greater complexity of the implementation and the need to adjust learning rates (η_w, η_a, η_b).

5.6 Comparative Conclusion

Overall, the results show that the **PID-Wavenet with the IIR filter** offers superior performance in accuracy, stability, and energy efficiency.

Although classic PID is suitable for steady-state conditions, the wavelet network-based approach demonstrates a better ability to adapt to variable evaporator conditions, maintaining $T_e(t)$ around the reference $T_{ref} = 10\,^{\circ}\mathrm{C}$ with minimal oscillation and no overshoot.

Consequently, PID-Wavenet control is considered the most robust and efficient strategy for nonlinear thermal systems, validating the experimental and numerical results reported in [11,25,26].

5.7 Practical Implications and Future Applications

It is acknowledged that the primary limitation of this work is the absence of experimental validation on a physical test bench. Real-world refrigeration systems are subject to unmodeled dynamics, such as sensor noise, actuator delays, and spatial gradients not fully captured by lumped-parameter models. However, the simulation results presented explicitly address these expected physical constraints through the design of the control architecture itself. Specifically, the integration of the IIR filter is a proactive measure designed to mitigate the measurement noise inherent in real sensors, which often destabilizes adaptive gains. Therefore, the numerical validation provided here constitutes a necessary and rigorous first phase, justifying the subsequent implementation of the PID-Wavenet in a Hardware-in-the-Loop (HIL) or experimental prototype scenario as the immediate next step in this research line.

The model and the results obtained allow us to visualize practical applications of PID-Wavenet control in small- and medium-scale thermal and refrigeration systems. The controller's ability to adjust its gains in real time makes it especially suitable for scenarios where thermal conditions are variable or uncertain, as occurs in:

- Intelligent refrigeration systems with variable frequency drive (VFD) compressor control.
- Liquid chillers used in laboratories or data centers.
- Compact HVAC systems and cold storage rooms with rapid temperature fluctuations.
- Experimental heat transfer test benches with automated thermal control.

From an applied engineering perspective, the incorporation of the IIR filter within the adaptive scheme improves control stability and reduces the computational effort of the Wavenet network, making its implementation viable in low-cost embedded controllers or real-time digital control systems (DSP or industrial microcontrollers).

In the future, this model can be extended to:

- Thermal management systems in unmanned aircraft (UAVs) or satellites, where heat dissipation depends on changing environmental conditions.
- Adaptive thermal control in hybrid air-liquid systems or in cooling modules for aeronautical power electronics.
- Integration with predictive algorithms based on deep neural networks or hybrid fuzzy-adaptive control models to optimize overall energy efficiency.

In conclusion, the results obtained validate the viability of PID-Wavenet control with an IIR filter as an innovative alternative to advanced thermal control, offering a balance between precision, robustness, and computational efficiency, with broad applications possibilities in thermal engineering, mechatronics, and aerospace.

Acknowledgement: We would like to express our sincere gratitude to Universidad Politécnica Metropolitana de Hidalgo for its support in equipment and financing the publication costs.

Funding Statement: The authors received no specific funding for this study.

Author Contributions: The authors confirm contribution to the paper as follows: Conceptualization, M. A. Vega Navarrete; methodology, L. E. Marron Ramirez, E. A. Islas Narvaez; software, M. A. Vega Navarrete; formal analysis, L. E. Marron Ramirez; investigation, C. M. Rodriguez Roman, P. J. Argumedo Teuffer; writing—original draft preparation, M. A. Vega Navarrete, C. M. Rodriguez Roman; writing—review and editing, C. M. Rodriguez Roman, P. J. Argumedo Teuffer. All authors reviewed and approved the final version of the manuscript.

Availability of Data and Materials: The datasets generated and analyzed during the current study are available from the corresponding author, upon reasonable request.

Ethics Approval: Not applicable.

Conflicts of Interest: The authors declare no conflicts of interest.

References

1. Gruhle WD, Isermann R. Modeling and control of a refrigerant evaporator. J Dyn Syst Meas Control. 1985;107(4):235–40. doi:10.1115/1.3140728.
2. Saxon A, Yang C, Santhanagopalan S, Keyser M, Colclasure A. Li-ion battery thermal characterization for thermal management design. Batteries. 2024;10(4):136. doi:10.3390/batteries10040136.
3. Young BR. Modelling and identification of a climbing film evaporator [dissertation]. Christchurch, New Zealand: University of Canterbury; 1992.
4. Mansour MK, Hassab MA. Novel lumped modeling for determining thermal performance of DX evaporator under partially-wet and fully-wet conditions. Appl Therm Eng. 2016;98:1025–35. doi:10.1016/j.applthermaleng.2015.12.094.
5. Kim D, Lee J, Do S, Mago PJ, Lee KH, Cho H. Energy modeling and model predictive control for HVAC in buildings: a review of current research trends. Energies. 2022;15(19):7231. doi:10.3390/en15197231.
6. Kam KM, Tadé MO. Simulated nonlinear control studies of five-effect evaporator models. Comput Chem Eng. 2000;23(11–12):1795–1810. doi:10.1016/s0098-1354(00)00291-x.
7. To LC, Tadé MO, Kraetzl M, Le Page GP. Nonlinear control of a simulated industrial evaporation process. J Process Control. 1995;5(3):173–82. doi:10.1016/0959-1524(94)00001-s.
8. Canela-Sanchez IJ, Juarez-Romero D, Escobar-Jimenez RF. Modeling and simulation of a helical falling film evaporator to improve its performance and design. Appl Ther Eng. 2023;228:120445. doi:10.1016/j.applthermaleng.2023.120445.

9. Bojnourd FM, Fanaei MA, Zohreie H. Mathematical modelling and dynamic simulation of multi-effect falling-film evaporator for milk powder production. Math Comput Model Dyn Syst. 2015;21(4):336–58. doi:10.1080/13873954.2014.980276.
10. Smith PD. Control and optimization of a multiple-effect evaporator. 2000 [cited 2025 Nov 12]. Available from: https://open.uct.ac.za/items/59a5b506-a2df-40ff-9d3e-48ed8d47a95d.
11. Vega S, Bravo M, Camacho O. A dual-adaptive PID control approach for nonlinear processes with variable parameters. In: Proceedings of the 2024 IEEE Biennial Congress of Argentina (ARGENCON); 2024 Sep 18–20; San Nicolás de los Arroyos, Argentina. p. 1–6. doi:10.1109/ARGENCON62399.2024.10735929.
12. Wang K, Zhang X, Bai L. Wavelet neural network control system based on fuzzy PID. Academic J Comput Inf Sci. 2021;2021(3):18–24. doi:10.25236/ajcis.2021.040303.
13. Jahedi G, Ardehali MM. Wavelet based artificial neural network applied for energy efficiency enhancement of decoupled HVAC system. Energy Convers Manag. 2012;54(1):47–56. doi:10.1016/j.enconman.2011.10.005.
14. Khan MAS, Rahman MA. A novel neuro-wavelet-based self-tuned wavelet controller for IPM motor drives. IEEE Trans Ind Appl. 2010;46(3):1194–1203. doi:10.1109/tia.2010.2045213.
15. Kanungo A, Choubey C, Gupta V, Kumar P, Kumar N. Design of an intelligent wavelet-based fuzzy adaptive PID control for brushless motor. Multimed Tools Appl. 2023;82(21):33203–23. doi:10.1007/s11042-023-14872-6.
16. Liu Z, Gao H, Yu X, Lin W, Qiu J, Rodriguez-Andina JJ, et al. B-spline wavelet neural-network-based adaptive control for linear-motor-driven systems via a novel gradient descent algorithm. IEEE Trans Ind Electron. 2024;71:1896–905. doi:10.1109/TIE.2023.3260318.
17. Castro J, Farnós J, Papakokkinos G, Zheng J, Oliet C. Transient model for the development of an air-cooled LiBr-H_2O absorption chiller based on heat and mass transfer empirical correlations. Int J Refrig. 2020;120:406–19. doi:10.1016/j.ijrefrig.2020.08.030.
18. Camacho EF, Gallego AJ, Escaño JM, Sánchez AJ. Hybrid nonlinear MPC of a solar cooling plant. Energies. 2019;12(14):2723. doi:10.3390/en12142723.
19. Saleh B, Aly AA, Alsehli M, Elfasakhany A, Bassuoni MM. Performance analysis and working fluid selection for single and two stages vapor compression refrigeration cycles. Processes. 2020;8(9):1017. doi:10.3390/pr8091017.
20. Bergman TL, Lavine AS, Incropera FP, De Witt DP. Fundamentals of heat and mass transfer. 8th ed. Hoboken, NJ, USA: Wiley; 2018. p. 992.
21. Kakaç S, Yüncü H. Heat exchangers: selection, rating, and thermal design. 2nd ed. Boca Raton, FL, USA: CRC Press; 2002. 520 p.
22. Dossat RJ, Horan TJ. Principles of refrigeration. 5th ed. Upper Saddle River, NJ, USA: Prentice Hall; 2002. 454 p.
23. ASHRAE. ASHRAE handbook: HVAC systems and equipment. Atlanta, GA, USA: American Society of Heating, Refrigerating and Air-Conditioning Engineers; 2016.
24. Stoecker WF, Jones JW. Refrigeration and air conditioning. 2nd ed. New York, NY, USA: McGraw-Hill; 1982.
25. Ramos-Velasco LE, Parra-Vega V, García Rodríguez R, Vega Navarrete MA. Knowledge-based self-tuning of PID control gains for continuum soft robots. Eng Appl Artif Intell. 2024;133(7):108447. doi:10.1016/j.engappai.2024.108447.
26. Garcia-Castro OF, Ramos-Velasco LE, Garcia-Rodriguez R, Vega-Navarrete MA, Escamilla-Hernández E, Oliva-Moreno LN. Estudio comparativo de controladores PID WaveNet-IIR aplicado a un helicóptero de 2 GDL. Pädi Boletín Científico De Ciencias Básicas E Ingenierías Del ICBI. 2022;10:36–42. doi:10.29057/icbi.v10iEspecial5.10067.
27. Proakis JG, Manolakis DG. Digital signal processing: principles, algorithms, and applications. 5th ed. Upper Saddle River, NJ, USA: Pearson; 2021. 1146 p.
28. Ogata K. Discrete-time control systems. 2nd ed. Upper Saddle River, NJ, USA: Prentice Hall; 1995. 776 p.
29. Domínguez CR, Espejel Rivera MA, Ramos Velasco LE, Ramos Fernández JC, Escamilla Hernández E. Wavelet neural network algorithms with applications in approximation signals. In: Batyrshin I, Sidorov G, editors. Advances in soft computing. Berlin/Heidelberg, Germany: Springer; 2011. p. 374–85. doi:10.1007/978-3-642-25330-0_33.